Review of Scientific Instruments ARTICLE scitation.org/journal/rsi

A new internally heated diamond anvil cell system for time-resolved optical and x-ray measurements

Cite as: Rev. Sci. Instrum. 91, 085114 (2020); doi: 10.1063/5.0009506
Submitted: 1 April 2020 • Accepted: 2 August 2020 •
Published Online: 20 August 2020

Yimin Mijiti,[1,2,a] Marco Perri,[1] Jean Coquet,[2] Lucie Nataf,[2] Marco Minicucci,[1] Angela Trapananti,[1] Tetsuo Irifune,[3] Francois Baudelet,[1,b] and Andrea Di Cicco[1,c]

AFFILIATIONS

[1] Physics Division, School of Science and Technology, University of Camerino, Via Madonna Delle Carceri 9, Camerino (MC) 62032, Italy
[2] Synchrotron SOLEIL, L'Orme des Merisiers, Saint-Aubin, BP 48, 91192 Gif-sur-Yvette Cedex, France
[3] Geodynamics Research Center, Ehime University, Matsuyama 790-8577, Japan

[a] **Author to whom correspondence should be addressed:** emin.mijiti@unicam.it
[b] **Electronic mail:** francois.baudelet@synchrotron-soleil.fr
[c] **Electronic mail:** andrea.dicicco@unicam.it

ABSTRACT

We have developed a new internally heated diamond anvil cell (DAC) system for *in situ* high-pressure and high-temperature x-ray and optical experiments. We have adopted a self-heating W/Re gasket design allowing for both sample confinement and heating. This solution has been seldom used in the past but proved to be very efficient to reduce the size of the heating spot near the sample region, improving heating and cooling rates as compared to other resistive heating strategies. The system has been widely tested under high-temperature conditions by performing several thermal emission measurements. A robust relationship between electric power and average sample temperature inside the DAC has been established up to about 1500 K by a measurement campaign on different simple substances. A micro-Raman spectrometer was used for various *in situ* optical measurements and allowed us to map the temperature distribution of the sample. The distribution resulted to be uniform within the typical uncertainty of these measurements (5% at 1000 K). The high-temperature performances of the DAC were also verified in a series of XAS (x-ray absorption spectroscopy) experiments using both nano-polycrystalline and single-crystal diamond anvils. XAS measurements of germanium at 3.5 GPa were obtained in the 300 K–1300 K range, studying the melting transition and nucleation to the crystal phase. The achievable heating and cooling rates of the DAC were studied exploiting a XAS dispersive setup, collecting series of near-edge XAS spectra with sub-second time resolution. An original XAS-based dynamical temperature calibration procedure was developed and used to monitor the sample and diamond temperatures during the application of constant power cycles, indicating that heating and cooling rates in the 100 K/s range can be easily achieved using this device.

I. INTRODUCTION

At present, most of the static high-pressure experiments are performed using large volume (such as Paris–Edinburgh or multi-anvil types) or diamond anvil cells (DACs). The large volume cell (LVC) apparatus can routinely reach pressures up to 30 GPa[1,2] using tungsten carbide (WC) anvils. Diamond anvil cells (DACs) are usually equipped with single-crystal diamond anvils and can reach ultra high static pressure up to hundreds of GPa.[3–6] The very good transparency of diamond anvils in a wide range of the electromagnetic spectrum allows investigation of compressed matter by means of various optical and x-ray based techniques and made DACs very successful and popular over the last decades.

Both LVC and DACs can be operated in a wide temperature range using different cryogenic or heating methods. In particular, high-temperature (HT) performances were explored in view

of the importance of laboratory measurements under the typical extreme conditions of geophysical interest. LVC heating techniques were developed earning their reputation in achieving homogeneous high temperatures up to 2000 K–3000 K.[7] They were used for *in situ* x-ray experiments mostly at pressures below 10 GPa (see Refs. 8–11 and references therein). High temperatures in LVCs are usually achieved through a resistive furnace enclosing the sample, and heating/cooling rates are affected by the large mass of the anvils that are in contact with the sample assembly. Several breakthroughs in DAC techniques instead have led to reach very high temperatures exceeding 6000 K[12–16] at ultrahigh static pressures. However, depending on the chosen methods for DAC heating, there are issues about heating/cooling rates, temperature gradients, and fine control.

High temperatures in diamond anvil cells are currently achieved by different strategies including laser heating, external or internal resistive heating techniques. Laser heating is especially used for achieving very high temperatures and is performed by means of an intense laser spot hitting a portion of the sample so that the local temperature is usually measured by means of spectral radiometry. There are known complications in applying laser heating for experiments at moderate temperatures (T < 1000 K). A known issue is that the local laser–sample interaction gives rise to considerably large temperature gradients across the hot spot.[17,18] Moreover, the sample itself should be able to absorb the incident laser beam, or a heat absorber has to be loaded in the sample chamber leading to possible mutual chemical reactions. Recent progress in the technique including double side heating and adjusting the laser into multi-mode and flat-top laser geometry helped to minimize the temperature gradients.[19,20] Another advantage of the laser heating technique is its potential for time-resolved rapid heating–cooling experiments using pulsed lasers,[21] avoiding major risks regarding cell and diamond integrity. However, it is still difficult to exploit laser heating in most time-resolved characterization techniques due to the dimensions of the hot spot and collection statistics. For example, for time-resolved x-ray absorption spectroscopy measurements in typical dispersive x-ray absorption spectroscopy (XAS) beamlines as in the case of ODE (Soleil Synchrotron),[22] the x-ray beam size is usually of the order of 30 μm–70 μm.

Currently, DAC experiments in the moderate HT range (T < 1500 K) are mostly performed using resistive heaters allowing for precise temperature control. In those experiments, the temperature can be reasonably estimated using thermocouples and calibrating power-temperature relationships. An external resistive heater is a relatively simple and easier solution, which heats the whole cell body by coiled wires surrounding the DAC and thus having a intrinsically slow heating/cooling rate and can be used up to 900 K.[23] Internal resistive heaters allow reaching higher temperatures up to 1500 K and are usually arranged inside the cell around the vicinity of the anvils, gasket, and/or the sample chamber, concentrating the heating spot in the sample region. However, most of the internal heating designs[24–28] are complicated due the need of arranging complex heating assemblies and temperature readout in a narrow DAC space and are seldom used routinely in high-pressure experiments. On the other hand, simpler internal heating schemes based on direct resistive heating of strip metallic gaskets have been proposed and tested in the past,[29,30] although never used for *in situ* spectroscopy experiments to the best of our knowledge.

In this paper, we present a new DAC setup including the gas membrane cell and a portable vacuum chamber allowing for a combination of *in situ* optical and x-ray experiments at high pressures and temperatures. The heating technique is based on suitably shaped W–Re alloy gaskets used as resistive elements, similarly to what was proposed in a previous publication[30] using different gasket materials and DACs. The DAC setup was conceived to achieve relatively fast heating/cooling rates, which can be applied for time-resolved *in situ* HT experiments. Full details of the design and thermal characterization of the performances are presented. We also present applications of this device for static and kinetic XAS measurements.

II. DESIGN OF THE INTERNALLY HEATABLE DAC

A. Features of the diamond anvil cell

The high-temperature DAC shown in Figs. 1(a) and 1(b) is a commercial cell (BETSA company, France, website: www.betsa.fr) made of Inconel. Typical sample pressures up to 100 GPa can be reached using this cell, depending on the size of anvil culets. The cell was conceived to allow both radial access [see Fig. 1(b)], mainly for the heating elements, and a wide angular aperture of about 75° for optical and x-ray spectroscopy purposes. In principle, any DAC (made by HT resistant materials) with enough radial access is adoptable for the internal heating described in this paper. The cell was equipped with type IIa diamond anvils (culet: 0.3 mm, height: 1.8 mm, and diameter: 3.4 mm) with ultra low fluorescence for the initial tests, optical data measurements, and selected x-ray measurements. Nano-polycrystalline diamond anvils[31] were also used in some cases for XAS measurements in order to get glitch free data in a broad photon energy range. Diamond seats made out of either TiB_2 or zirconia were used in different experiments. Due to its very good thermal insulation property, zirconia was found to be a suitable seat material for very high-temperature measurements, increasing the heating efficiency by significantly decreasing the power required to achieve high temperature. In our experiments, the diamond anvils were kept in place on their seats using a HT glue (Pyrofeu® Ref. 4928), although high-precision mechanical positioning system are certainly an option for future designs.

B. Internal heating

Most of the DAC internal heaters are complicated by the internal geometry and small size of the sample, which may imply the use of small electrical wires to carry the heating current that is usually quite large for reaching high temperatures by the Joule effect. The limited adoption of internal heaters as a tool for routine HT experiments under high pressure can be also assigned to the use of complex and fragile heating elements. Several solutions have been proposed in the past, such as alumina-coated wires in touch with the metallic gasket surrounding the sample or a small electrically insulated cylindrical oven surrounding and radiatively heating the diamonds. In a previous work, we have also reported another development for the internal heating element that was based on a conveniently shaped graphite foil surrounding the sample region,[32] similarly to what was proposed and already successfully used by other researchers (see Ref. 27 and references therein). However, those strategies still require major efforts and care in preparing the sample assembly

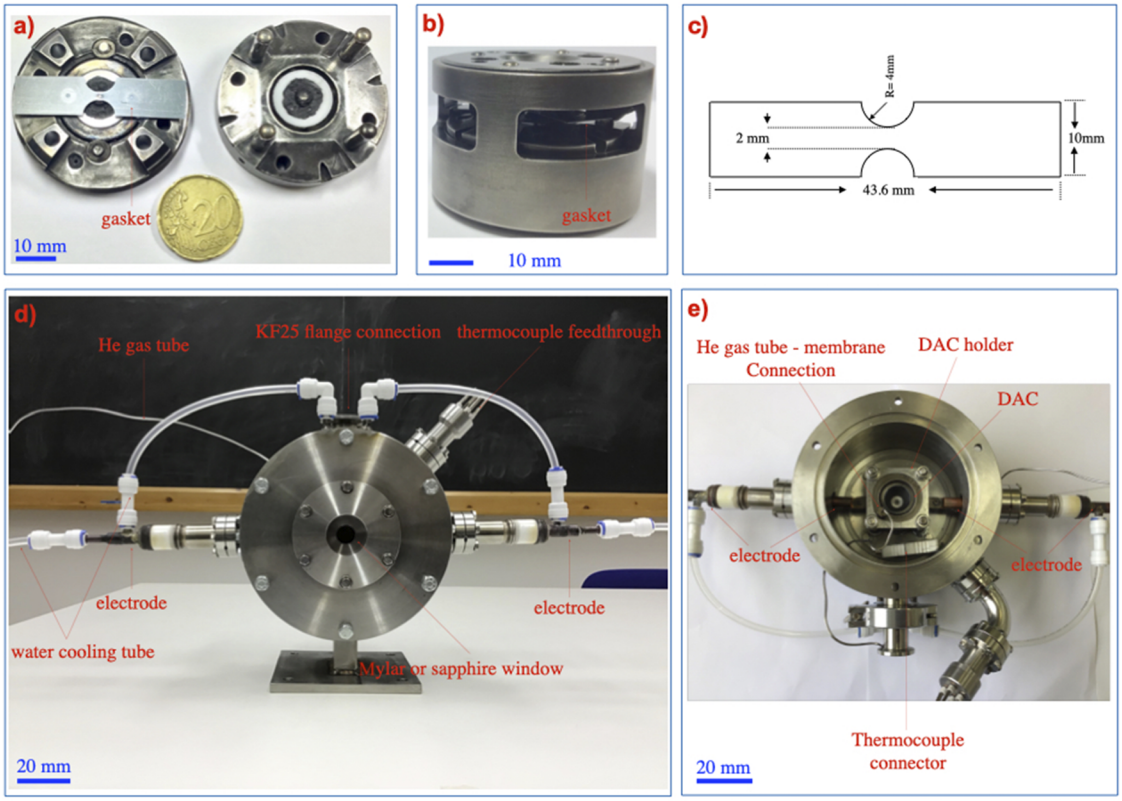

FIG. 1. (a) Internal view of the internally heatable DAC showing the self-heating gasket and major DAC components. (b) Side view of the radial access of the assembled DAC. (c) Design of the gasket used also as the heating element. External (d) and internal (e) views showing the design and main components of the vacuum chamber developed for high-temperature measurements using the DAC.

and resulted to be difficult for performance of routine high-pressure experiments using reliable temperature calibrations.

The internal heating strategy pursued in this work is similar to the one already presented by Balzaretti *et al.*[30] and was intended to provide (i) a clean, simple, and reliable solution for optical and x-ray high-temperature measurements with a DAC and (ii) a device suitable for well-characterized time-resolved XAS experiments (within the typical timescales of the XAS dispersive setup). The particular shape of the metal gasket, as shown in Figs. 1(a) and 1(c), is similar to that chosen for crucibles in other high-temperature applications.[30,32–34] It was designed in order to limit the total supplied power and deliver the heat directly at the central region where the gasket is indented, drilled, and filled with the sample. For those heaters, the expected temperature distribution for an applied external voltage shows a high-temperature plateau only in the central region. In addition, direct connection with the electrodes takes place at the opposite edges of the gasket (distance of about 43.6 mm) that are kept at moderate temperatures and placed externally of the DAC, avoiding complicated connections inside the limited space of the DAC.

A W–Re (25% Re) alloy was selected as a suitable low-cost gasket material considering its excellent high-temperature performances, good electrical resistivity, and mechanical stability properties. This tungsten-based material was not tested previously (see Ref. 30 in which Inconel, Ta, and Rh/Mo alloy were used) and proved to be very efficient for high-temperature measurements. Gaskets made by this type of alloys were used safely in high-pressure experiments up to 100 GPa and 1200 K.[24] Here, gasket thickness was set to 150 μm allowing for both sample confinement and heating using limited electric currents (0 A–60 A). In this work, we have successfully used self-heating gaskets made by this material, although we noticed that it could be subject to deformations at higher temperatures resulting in pressure drifts especially in the first quasi-isobaric heating cycle. In principle, this issue can be solved by using other gasket materials with higher temperature strength and/or by inserting amorphous boron epoxy, cubic boron nitride epoxy, or diamond powder epoxy rings into the sample chamber. The latter method was successfully used in previous resistive heating DAC experiments to reinforce the Re gasket at high temperature.[35,36]

C. Vacuum chamber

As it is well known, DAC high-pressure experiments at temperatures higher than ~700 K require controlled inert atmosphere

surrounding the active components of the cell including the diamonds. In this work, we have developed a suitable vacuum chamber conceived to prevent the deterioration of diamond anvils and oxidation of the metallic gasket as well as other cell components at high temperatures. The vacuum chamber was designed (see also the supplementary material) to allow the performance of different optical and x-ray experiments such as x-ray diffraction as well as x-ray absorption and Raman spectroscopy. The aim of the design was to obtain the most compact and versatile chamber to be installed in different experimental setups including laboratory optical/x-ray spectrometers and synchrotron radiation beamlines.

The stainless steel vacuum chamber containing the DAC heating assembly is shown in Figs. 1(d) and 1(e). The vacuum chamber was designed considering all the necessary feedthroughs and view ports for diagnostics and for using x-ray and/or optical probes. Easy interchangeable window materials have been conceived and used for x-ray and optical experiments. Thin Kapton and Mylar windows were used for incoming and outgoing synchrotron radiation x-ray beams, while a sapphire window was used for optical measurements. One of the windows was designed to be close enough to the cell so that the minimal distance from the sample is compatible with long-distance microscope objectives. The distance between the external surface of the window and the sample was kept lower than 20 mm, compatible, for example, with the 20× lens used in the optical experiments reported in this work (focal distance 25 mm). Optical windows were used for detecting the ruby fluorescence (pressure gauge), Raman, and thermal emission signals in laboratory experiments. Mylar windows allowed performance of x-ray experiments and collection of the ruby fluorescence signal for determination of the internal pressure. We have kept the vacuum within 10^{-3} mbar or less in order to avoid deterioration of the diamond anvils and other metal parts at high temperature.

The heating element (self-heating gasket) was conceived in order to be tightly connected to the copper electrodes near to the cell cylinder, ensuring an efficient electric current flow. Both electrodes and optical windows have been designed to be water-cooled to guarantee longer heating runs at very high temperatures, as shown in Figs. 1(d) and 1(e). In present experiments, the electrical power was provided by a Delta SM15-200D power supply usually operating in a range of currents and power not exceeding 60 A and 120 W, respectively. During the various tests under high-temperature conditions, we have verified that the body of the cell never exceeded temperatures higher than 500 K (60 min of continuous heating) for typical sample temperatures around 1200 K. Accurate measurements of the local sample temperatures were done using specific techniques, as described in Sec. III.

III. TEMPERATURE DISTRIBUTION AT HIGH PRESSURE

Accurate measurement of the local sample temperature is an important issue for HT experiments with the diamond anvil cells. Measurements of high temperatures under high pressure are often performed analyzing the thermal emission signal, a technique commonly used in association with laser heating. This technique allows for direct measurements of the sample temperature inside the DAC with micrometric spatial resolution when suitable collection optics are used. Of course, thermal emission measurements can be also used for local temperature estimation in resistive heating DACs, within temperature ranges depending on the sensitivity and detectable wavelength range of the optical spectrometer. In this work, we have carefully tested the performances of the DAC by using mainly thermal emission measurements, establishing also a robust electric power-temperature relationship for the self-heating gasket (and diamond-seat assembly) under consideration.

A. Temperature measurements

The heatable DAC described above allows easy optical access to the sample, thus enabling us to evaluate the local temperature and heating characteristics by analyzing the thermal emission signal, which is known to follow the Planck black-body distribution for a given emissivity. For this work, we have exploited a micro-Raman setup combining an open-space confocal microscope Olympus BXFM with a suitable long-distance objective (Olympus SLMPlan 20× objective, with 25 mm working distance), connected through optical fibers to an optical spectrometer (HORIBA, iHR320). This setup allowed us to perform combined experiments measuring the ruby emission line excited by a green laser (solid-state 523 nm, 50 mW) for pressure determination and the thermal emission signals at high temperature (obtained switching off the laser source and removing the necessary optical filters for Raman spectroscopy). Of course, Raman scattering experiments under high pressure and temperature conditions are possible with the same setup and were occasionally performed. Different gratings were used for thermal emission and Raman spectra (600 lines/mm and 1800 lines/mm, respectively), while the necessary broad spectral coverage and efficient photon counting was obtained by a scientific grade Peltier-cooled CCD (Horiba Sincerity).

Thermal emission measurements have been shown to provide precise estimations of the local temperature of the sample inside the DAC (see the supplementary material for details). Thermal emission measurements presented in this work were obtained with large integration times (1 min–20 min) depending on the injected electrical power and refer to the equilibrium temperatures (thermal equilibrium is approached usually within 1 min, as shown in Sec. IV B). In most cases, the local sample temperature at thermal equilibrium can also be conveniently estimated by using suitable calibration curves expressing the relationship between the injected electric power and the temperature, for a given heating gasket geometry. We have thus carried out a series of experiments aimed to determine such a relationship using basically two probes for the local temperature: the established radiospectrometry technique (see the supplementary material) for T > 800 K and the known temperature dependent ruby fluorescence line shift[37] for T < 850 K. A type-K thermocouple of diameter 0.25 mm was also attached near the center of the heater gasket, keeping track of the temperature of the gasket. However, temperature readout was found dependent on the positioning and was not well reproducible for different heating runs, with typical fluctuations above 10%. We expect that attaching the thermocouple to the pavilion or back side of the diamond anvil may provide better reproducibility with a slight systematic deviation with respect to the sample temperature[24] due to the fact that temperature gradients on the diamond surface can be smaller because of its high thermal conductivity.

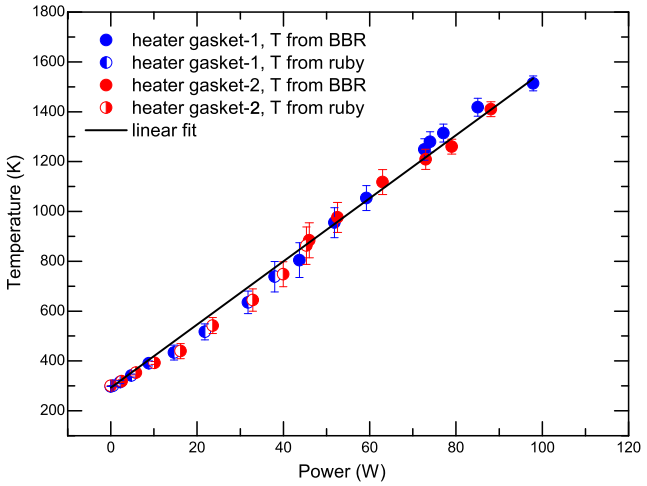

FIG. 2. Local temperature for various values of supplied power, measured in separate heating runs, which were performed with two different heating gaskets (gasket-1, gasket-2) of identical geometry. For T > 800 K, temperatures were measured by thermal emission measurements [black-body radiation (BBR)] and are shown as filled circular dots. For T < 850 K, temperatures were measured using the ruby fluorescence signal and are represented by half-filled circles. The solid black line represents a linear fit.

The results for two different heating experiments of a Ge sample inside the DAC are reported in Fig. 2. For those experiments, the anvils were pressed onto the gasket, and the sample chamber was closed cautiously resulting in an internal pressure near 1 bar. The two separate runs cover the 300 K–1500 K temperature range for a maximum input power of about 100 W and are in nice agreement among themselves. The power–temperature relationship has been found to follow quite closely a linear trend in the 800 K–1500 K range as measured by thermal emission, as expected. A slight deviation from linearity is observed at around 800 K range when matching the temperature measurements obtained by the ruby fluorescence wavelength shift. This may be assigned to systematic deviations between the two scales and to the known difficulties (broadening) in using the ruby scale at high temperatures.

Nevertheless, the results shown in Fig. 2 indicate that a nearly linear and reproducible relationship exists among electric power and temperature, which can be safely used for a given class of heatable gaskets of identical shape and the same diamond-seat assembly. Therefore, for a given sample assembly, such a power–temperature relationship can be established prior to real experiments and can be applied for temperature estimations in multiple sample loadings and heating runs. We have verified that the same curve can be applied also at moderately high pressures (up to about 10 GPa). As an example, the data reported in Fig. 2 were interpolated by a linear function: $T(K) = 293 + 12.663\,25 \times P(W)$, which follows closely the temperature trend above 800 K and has been used as a reference in Sec. IV.

B. Temperature distribution and gradients

Spatial uniformity of the sample temperature is an important feature to be considered in high-temperature experiments with diamond anvil cells. The experimental setup described in Sec. III A

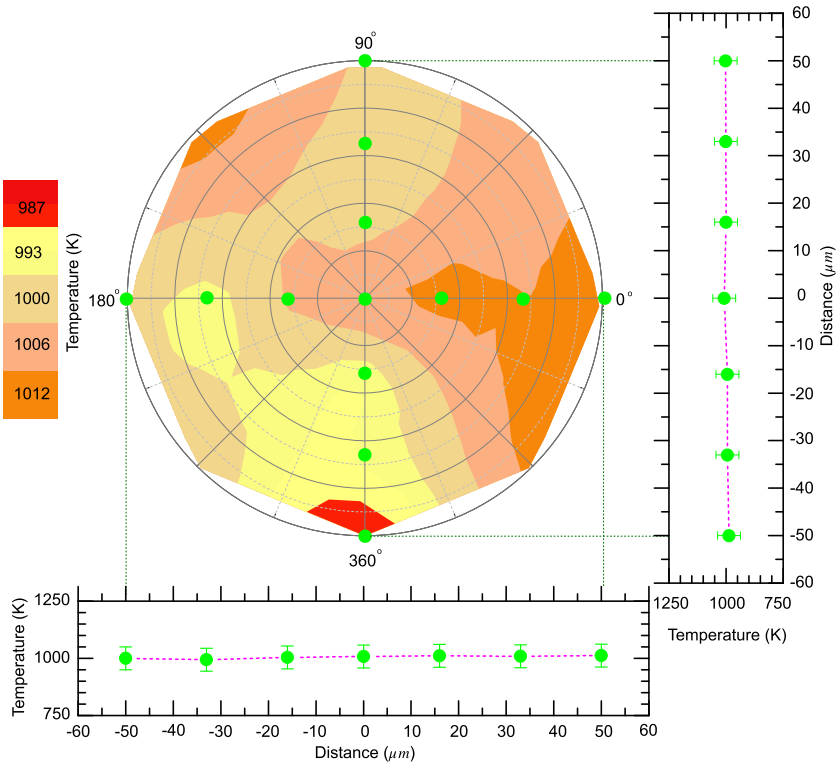

FIG. 3. 2D contour plot of the temperature distribution inside a 100 μm sample chamber filled with fine Ge:BN (mixture with 1:1 ratio) powders. Pressure was at P = 4.65 GPa, and temperature was stabilized at ~1000 K, just below the melting point at this pressure (~1020 K). Estimated temperatures at selected points along horizontal and vertical directions are shown in the insets (bottom and right side). Temperature gradients are found below the present accuracy in temperature determination.

allowed us accurate measurements of the thermal emission with a typical spatial resolution of 10 μm (the size of the focal spot of the 20× long-distance objective). We have thus performed a campaign of thermal emission measurements on different samples at various temperatures inside the DAC using an xy translation stage moving the DAC vacuum chamber with a typical step of 16 μm, covering the surface of the entire sample. In this way, we have been able to evaluate the temperature distribution of the pressurized sample and verify the occurrence of possible radial thermal gradients.

A typical result obtained during these experiments is shown in Fig. 3, where a 2D contour plot of the temperature distribution inside a 100 μm wide sample chamber is reported. In this example, the sample chamber was filled with a fine (submicrometric) powder mixture of Ge and BN (with 1:1 ratio). The pressurized sample at P = 4.65 GPa was heated and stabilized for a few minutes at an average temperature T ~ 1000 K (corresponding to an injected electrical power of 56 W), just below the melting point of Ge (~1020 K, see Fig. 4). Thermal emission spectra have been collected as reported in Sec. III A, by focusing the long distance 20× objective at different positions across the sample chamber.

Local temperatures associated with thermal emission signals related to different xy positions were evaluated, as discussed in Sec. III A. In Fig. 3, we have reported both the 2D temperature map and the obtained temperature axial profiles. Looking at Fig. 3, we can see that possible temperature gradients inside the cell are really limited, well below the estimated uncertainty on the measured temperature. In fact, temperature differences on the radial direction inside the sample chamber are less than 25 K, in the presence of a typical 50 K estimated standard deviation (5%). The longitudinal temperature profiles shown in the insets of Fig. 3 clearly show that temperature variations are within the estimated uncertainty (~5%). While it is difficult to obtain reliable data for the temperature distribution in the axial direction, we estimate that also those temperature gradients are negligible since the tiny and thin (few tens of μm) sample layer is heated in a cylindrical symmetric configuration by the gasket. Moreover, direct contact of both the gasket and the sample with the highly thermal conductive diamond anvils is thought to provide another source of thermal equilibrium in the sample chamber.

Based on those results, we can safely conclude that a very homogeneous temperature distribution can be achieved for a pressurized sample in the present internally heatable DAC device.

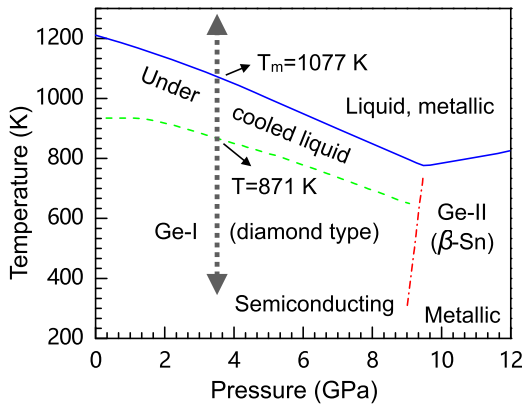

FIG. 4. Phase diagram of elemental Ge, as given in Ref. 10. Reported XAS data in this work were collected under isobaric conditions, along the dashed gray line at ~3.5 GPa. The melting temperature T_m at this pressure is ~1077 K.

IV. STATIC AND KINETIC XAS MEASUREMENTS

The new high-temperature DAC system has been successfully used for different optical and x-ray experiments. In particular, we have performed a series of XAS experiments on elemental germanium at variable temperatures with the specific purpose of assessing the performances of the heatable DAC for both static and time-resolved XAS measurements.

The sample for XAS measurements was obtained by mixing the fine powders of Ge and BN with 1:2 ratio and filling the predrilled sample chamber (of 120 μm diameter) in the W/Re25 heatable gasket. BN powders were used both as a pressure transmitting medium and to dilute the sample preventing also chemical reactions between molten Ge and the metallic gasket. In fact, sample-gasket reactions were observed upon melting for Ge samples in direct contact with the gasket. The use of the mixture allowed us the realization of several heating and cooling cycles before observations of gasket damages, without using sample-gasket separators in the sample chamber.

The pressure before and after the heating cycles was measured applying the standard ruby fluorescence technique. Ge K-edge XAS data were collected in dispersive geometry at the ODE beamline[22] of Synchrotron SOLEIL by focusing the photon beam in the sample region with an elliptically curved Si (111) crystal polychromator. Photon absorption at different photon energies was measured by using a position sensitive CCD detector. The pixel-energy calibration of the XAS data was performed using the L_2-edge XAS spectrum of Tantalum (Ta) foil measured at ambient conditions in the energy scanning mode. The setup of the ODE beamline was similar to that presented in Ref. 38, allowing for combined collection of XAS spectra with x-ray diffraction.

A. High-temperature Ge K-edge XAS under pressure

Elemental Ge is a semiconductor with a diamond-type structure in the Ge-I phase, as shown in the phase diagram reported in Fig. 4. Germanium (Ge-I) shows a peculiar melting behavior accompanied by drastic changes in the electronic and local atomic structure, with an increase in the coordination number from 4 to 6–7 and closure of the bandgap (metallization).[10,39,40] Therefore, melting of solid Ge-I at high temperature can be easily observed through optical observations or x-ray spectroscopy experiments, providing an ideal system to characterize the present HT DAC system. For example, the drastic increase in the optical reflectivity of Ge upon melting (metallization) can be easily observed for increasing pressures along the melting line of the phase diagram, as shown in the images in Fig. 5, for Ge at 1250 K and 300 K at ambient pressure (Ge melting point T_m = 1211.2 K).

The semiconductor–metal transition and coordination crossover upon melting are easily observable in the XAS features as well. Figure 6(a) presents a set of Ge K-edge XAS data measured

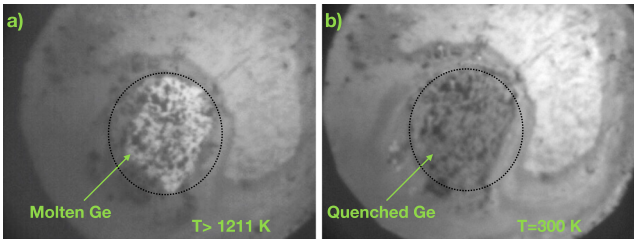

FIG. 5. Optical images of the molten (a) and melt quenched (b) Ge sample. The sample was not pressurized and has a melting point T_m = 1211.2 K.

at different static temperature conditions up to about 1280 K. The data were collected during slow heating and cooling cycles (approximate rate 100 K/min) performed with the presented HT DAC at a pressure of 3.4 GPa. As more clearly indicated in Fig. 6(b), the K-edge onset energy E_0 (defined as the maximum of the first derivative) shifts to lower energy values upon heating due to the effects of the lattice expansion and the progressive renormalization of the semiconducting bandgap by phonons.[41] When melting occurs, a step-like red shift of E_0 is observed (~1.5 eV as compared to the solid at 300 K) because of the drastic collapse of the electronic bandgap following the metallization. On the other hand, in addition to this drastic change in the electronic structure, the increase in the coordination number and corresponding changes of the short range order around the Ge atom results in clear changes of the near-edge XAS features, as shown in Fig. 6(c).

Interestingly, as can be seen in Figs. 6(a) and 6(b), the spectral features of the metallic liquid were preserved even below the melting line. This observation, corresponding to the occurrence of the undercooled liquid regime, was discussed in previous studies[40] using highly homogeneous and diluted (Ge:BN = 1:10 mixture) micrometric Ge droplets samples. Present data confirm the supercooling properties of liquid Ge under high pressure also using a different sample mixture (Ge:BN = 1:2). Generally speaking, the experimental results reported in Fig. 6 indicate that successful XAS experiments along static heating and cooling cycles (largely exceeding the Ge melting point T_m = 1077 K at 3.4 GPa) can be performed using the present internally heated DAC system.

B. XAS measurements of heating and cooling rates

Due to its technical design, the internal heating system is expected to show interesting performances regarding the achievable heating and cooling rates. In order to understand the limits of the achievable heating and cooling rates, we have performed a series of kinetic Ge K-edge XAS measurements of the above-mentioned mixture (Ge:BN = 1:2) using the typical sub-second time resolution allowed by the dispersive setup of the ODE beamline (synchrotron SOLEIL).[22] For these experiments conceived at high heating and cooling rates, we have used type 2a single-crystal diamond anvils (with 0.3 mm culet, 1.8 mm height, and 3.4 mm diameter) instead of

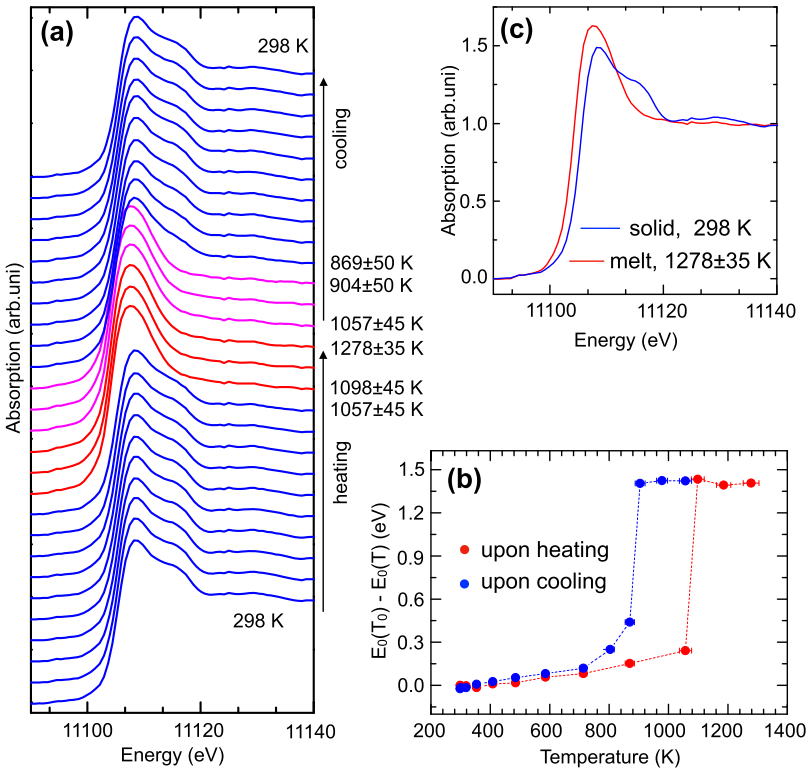

FIG. 6. (a) Ge K-edge XAS of elemental Ge measured at different temperatures during slow heating and cooling cycle, at pressure P = 3.4 GPa. XAS spectra for the solid, liquid, and supercooled liquid phases are represented by blue, red, and purple colors, respectively. (b) Shift of the edge energy $[E_0(T_0) - E_0(T)$, where T_0 is the initial temperature] at different temperatures upon heating and cooling. (c) Comparison of the typical Ge K-edge XAS for solid (Ge-I phase) and liquid Ge.

nano-polycrystalline (NPD) anvils, which allowed us also to collect information about temperature variations of the diamonds.

Figure 7 reports a set of time-resolved XAS data measured for a single heating/cooling cycle performed with a step-like rise/drop of the injected electric power (0 W–98 W, square wave). Here, we show only one thermal cycle, although we performed several experiments of the same kind with similar results (another set of data is reported in the supplementary material, see Figs. S11 and S12). In Fig. 7(a), we report the 2D plot of the measured XAS (color gradient scale on the right) as a function of the acquisition time and x-ray energy. The step-like time dependence of the supplied electric power is reported at the left side of the 2D XAS plot for easier understanding of the data measurement process. A single Ge K-edge XAS spectrum measured at time 0 (at room temperature) is also given in the lower part of the figure. XAS data of reasonable quality were collected with a 157 ms time resolution (including the detector dead time).

Kinetic XAS record of this experiment was started at t_0 = 0s, and finalized after 60.8s at t_f = 60.80s. The step-like function representing the action of the power supply is shown in the left side of Fig. 7(a). The power (98 W) supply was started (power supply on) at t_1 = 6.0 s, and terminated (power supply off) after 30 s at t_2 = 36.0 s. The applied electrical power (98 W) is known to correspond to a final equilibrium temperature T_{limit} = 1534 K, according to the established power–temperature relationships shown in Fig. 2.

As shown in Fig. 7(a), the XAS signal is strongly modulated by the temperature variations imposed to the sample as a function of time. In particular, the use of single-crystal diamond anvils is associated with the presence of several clear features (glitches) in the absorption spectrum due to the escape of photons from the detector sensitive area because of strong Bragg reflections. The position of these extra-absorption features has been found to be strongly dependent upon temperature (time) with parallel trends (an exemplary pre-edge glitch is indicated as G_1). Of course, the rapid temperature change is also reflected by the corresponding changes in the Ge K-edge XAS, especially near the edge energy onset E_0, although barely visible on the scale of Fig. 7(a). The time evolution of glitch G_1 (related to diamonds) and of the near-edge XAS features is better visualized in the enlarged 3D plot shown in Fig. 7(b).

The time-dependent patterns shown in Fig. 7(b) can be used for a detailed study of the temperature variations inside the DAC with the typical time resolution of the XAS spectra. In fact, on the one hand, we have a well-defined relationship among the temperature and edge energy (E_0) shift, as shown in Fig. 6(b). On the other hand, thermal expansion of the diamond, which is associated with the energy variations of the glitch G_1, can be found in the literature (see Ref. 42 and references therein). The time evolution of E_0 and G_1 here is assumed as representatives of the temperature variations of the sample and of the diamonds, respectively.

In Fig. 8(a), we show that the temperature dependence of edge energy [$E_0(T)$] reported in Fig. 6(b) (heating ramp) can be nicely represented up to the melting point (T_m) by a continuous second-order polynomial function ($T = T_0 + a\Delta E_0 + b\Delta E_0^2$, T_0 = 315K, a = 5441.85 K/eV, and b = −10 064.1 K/eV^2). The large shift of the onset edge energy E_0 upon melting (around 1.5 eV as compared to room temperature) can be used as a fingerprint for T_m. At temperatures above T_m, the fairly constant E_0 in the liquid phase does not allow reasonable temperature estimations for sample.

In Fig. 8(b), we replot the temperature vs diamond lattice constant data reported in the literature.[42] As it can be seen, the temperature vs diamond lattice constant data are well reproduced in the 300 K–1250 K range by a continuous polynomial function (blue line in figure): $T = T_0 + T_1 \times (a(T) - a_0) + T_2 \times (a(T) - a_0)^2 + T_3 \times (a(T) - a_0)^3 + T_4(a(T) - a_0)^4$, T_0 = 298 K, T_1 = 1.773 43 × 10^5 K/Å, T_2 = −2.513 37 × 10^7 K/Å^2, T_3 = 2.474 21 × 10^9 K/Å^3, and T_4 = −8.783 23 × 10^{10} K/Å^4, where a_0 = 3.567 12(2) Å (see Ref. 42 and references therein) is the lattice constant at T_0 = 298 K and ambient pressure for type IIa diamonds.

In Fig. 9(b), we report the variation of the Ge K-edge energy onset $E_0(t_0) - E_0(t)$ as a function of time. The gradual shift of the edge energy E_0 (defined as the maximum of the first derivative) for

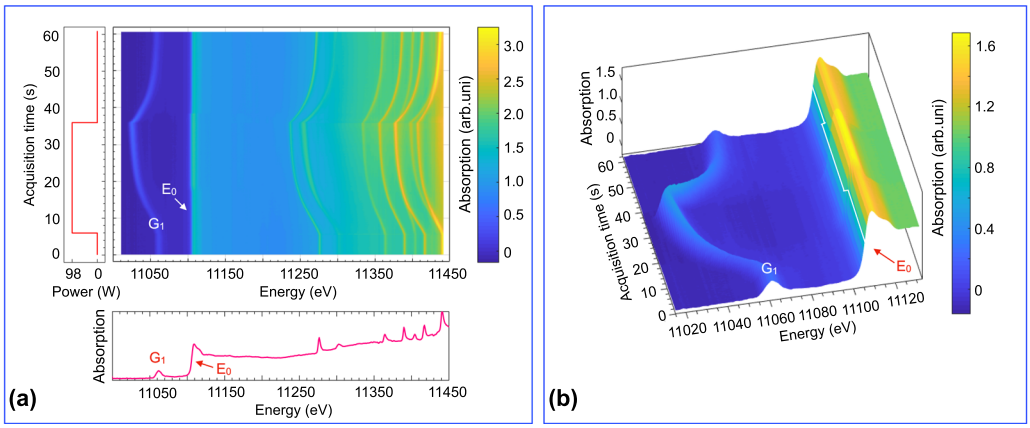

FIG. 7. (a) 2D plot of time-resolved Ge K-edge XAS data representing the absorption as a function of photon energy and acquisition time (t). For clarity, the supplied electric power as a function of time is reported in the left side of the figure (square wave). The Ge K-edge XAS spectrum at room temperature (t = 0 s) is shown at the bottom. (b) 3D visualization of time-dependent evolution of the near-edge XAS, including first diamond glitch (G_1). The whole set of data was measured kinetically at a nearly constant pressure P = 3.5 GPa.

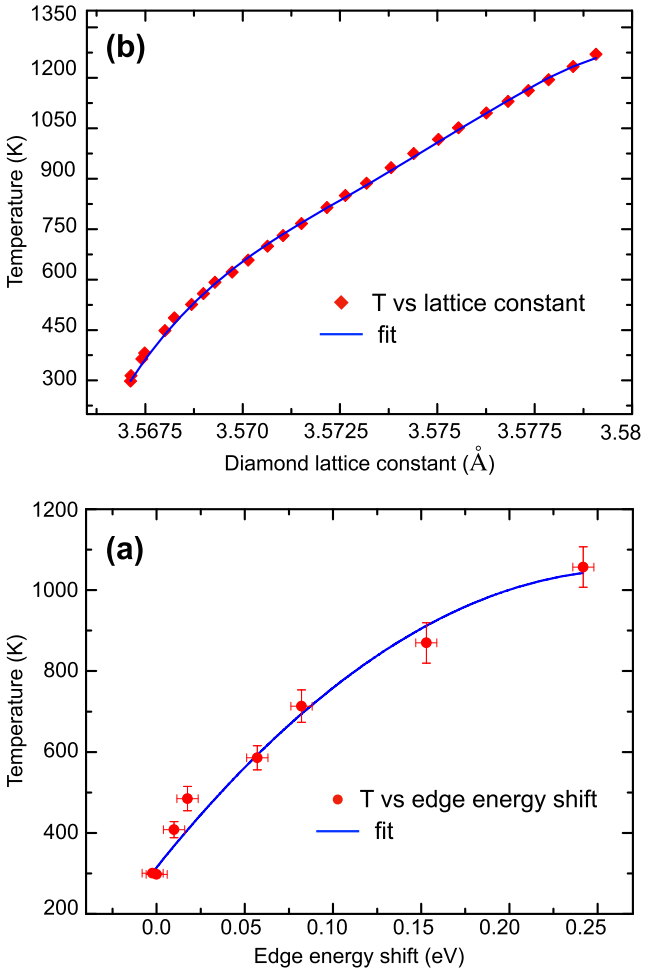

FIG. 8. (a) Sample temperature vs edge energy shift $\Delta E_0 = E_0(T_{RT}) - E_0(T)$ ($T_{RT} \sim 298$ K) upon heating in the static XAS experiment reported in Fig. 6. A second-order polynomial function (blue line) nicely interpolates the data up to the melting point. (b) Temperature vs diamond lattice constant a(T) according to Ref. 42, interpolated by a smooth fourth-order polynomial function (blue line, see text).

the solid Ge sample, and the subsequent melting process is clearly visible, following the application of the electrical power [Fig. 9(a)]. The sample temperature T(t) as a function of time has been obtained using the calibration curve in Fig. 8(a), and the results are reported in Fig. 9(c) for temperatures up to the melting point T_m (in the solid phase).

Although no precise information on temperature can be obtained by XAS data of liquid Ge, we can safely use the discontinuous change of the edge energy E_0 occurring at the solid–liquid transition (melting point) as a fingerprint of T_m. Melting of the entire Ge sample is seen to occur in less than 2 s, as measured by the time delay between the last point related to a pure solid phase ($t_3 = 16.8$ s) and the first point of the liquid with a stable onset edge energy shift $E_0(t_0) - E_0(t) \sim 1.5$ eV. Determination of the sample temperature upon cooling (times exceeding $t_2 = 36.0$ s) is complicated by the occurrence of supercooling of the liquid, which is indeed largely dependent on the size distribution of the Ge droplets in the BN matrix. In the present experiment, the nucleation of Ge droplets to a crystal phase is seen to occur in a rather short times (less than 0.5 s), as indicated by only a couple of $E_0(t_0) - E_0(t)$ points lying in the range between those typical of the liquid and of the solid. Sample temperature values can be reliably obtained only for times larger than $t_4 \sim 40$ s on the scale of Fig. 9(c).

In Fig. 9(d), we plot the time-dependent energy shift of glitch G_1 [$E_{G_1}(t_0) - E_{G_1}(t)$]. The energy variations of this feature are in nice correlation with the imposed electrical power [Fig. 9(a)] and are assumed to be associated with the thermal expansion of one of the diamonds. As shown in Fig. 7, we have observed very clear (sharp) features related to Bragg reflections at any temperature, indicating the occurrence of a homogeneous thermal expansion of the diamonds involved in the diffraction process. The absence of important temperature gradients is compatible with the exceptional thermal conductivity of the diamonds.

As discussed above, the thermal expansion of the diamond crystal lattice parameter a(T) is well studied in a wide temperature range.[42] The a(T) variation with temperature is obviously reflected on the inter-planar distances d(T) associated with diamond Bragg reflections realized at well-defined photon energies. Using single-crystal diamond anvils in the present experiment, the Bragg condition can be satisfied at certain x-ray energies. Consequently, transmittance of the x-ray photons at those energies will be affected generating glitch-like peaks in the absorption spectrum for a given photon energy E_G,

$$E_G(T) = \frac{nhc}{2\sin(\theta)} \cdot \frac{1}{d(T)}. \quad (1)$$

The temperature dependence of the Bragg reflection is just the inverse of that valid for the inter-planar distances d(T). In the fixed-geometry x-ray experiment described here, the coefficient $\frac{nhc}{2\sin(\theta)}$ is a constant (θ being the Bragg angle, h is the Planck constant, and c is the speed of light). In an isotropic system such as diamond, thermal expansion is applied to all interplanar distances d: $d(T)/d(T_0) = a(T)/a(T_0)$. The energy position $E_G(T_0)$ at the initial (room) temperature T_0 is known; therefore, neglecting possible variations of the thermal expansion in pressurized diamonds, we can easily evaluate the $a(T)/a(T_0)$ ratio corresponding to a given energy $E_G(T)$,

$$\frac{a(T)}{a(T_0)} = \frac{E_G(T_0)}{E_G(T)}. \quad (2)$$

We have been thus able to evaluate the diamond temperature T(t) as a function of time by applying Eq. (2) to the $E_{G1}(t)$ data reported in Fig. 9(d). Temperature conversion has been obtained using the a(T) calibration curve of Fig. 8(b), and the results are reported in Fig. 9(e) for all the temperatures under consideration.

The time evolutions of the sample and diamond temperatures [shown in Figs. 9(c) and 9(e)] can be well represented by exponential models, for both heating and cooling,

$$T(t)_{rise} = T_0 + (T_{limit} - T_0)(1 - e^{-(t-t_1)/\tau_1}), \quad (3)$$

$$T(t)_{decay} = T_f + (T_{max} - T_f)(e^{-(t-t_2)/\tau_2}), \quad (4)$$

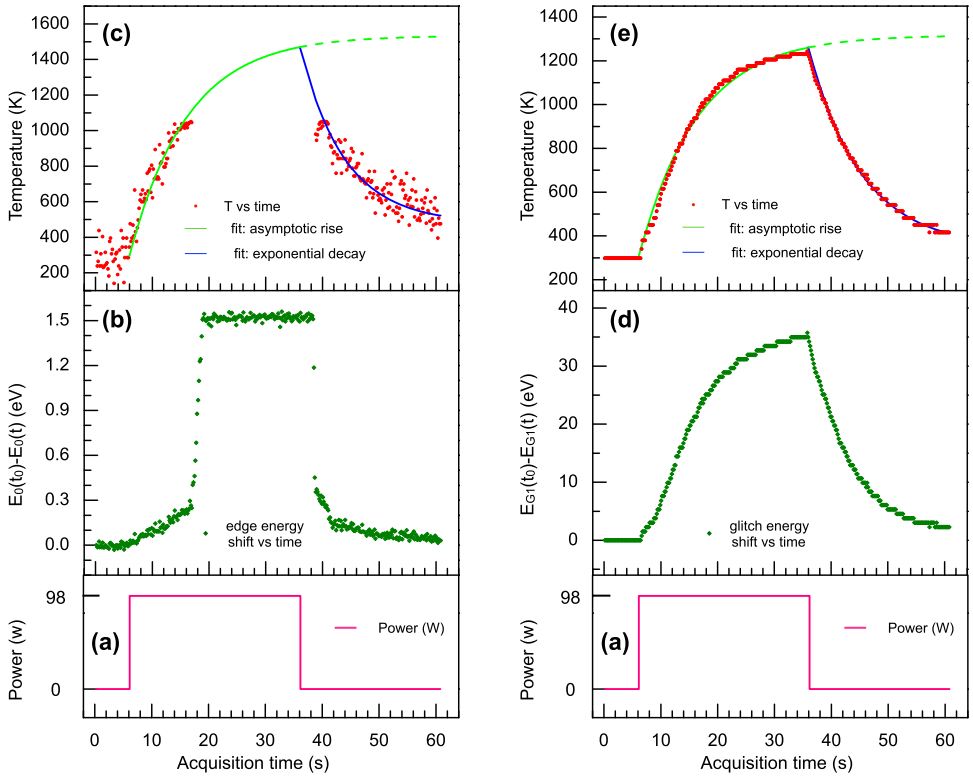

FIG. 9. (a) Time dependence of the electric power within the XAS data acquisition time. (b) Time evolution of the XAS edge energy shift: $E_0(t_0) - E_0(t)$. (c) Time evolution of the sample temperature obtained from the established relationship in Fig. 8(a). (d) Energy shift $[E_{G_1}(t = 0) - E_{G_1}(t)]$ of the diamond glitch G_1 as a function of time. (e) Time evolution of the average diamond temperature derived from the energy shift of the glitch G_1 [shown in (c)] using the relationship in Fig. 8(d). Time evolutions of the sample and diamond temperatures were represented by exponential models for both heating (green curves) and cooling (blue curves) process.

where τ_1 and τ_2 are the time constants for the heating (constant power) and cooling (no power) rates inside the DAC. Equation (3) is defined in the time region between $t_1 = 6.0$ s (power supply on) and $t_2 = 36.0$ s (power supply off), while T_0 and T_{limit} are the initial (ambient) and final temperature after a long equilibration time τ_h ($\tau_h \gg \tau_1$). On the other hand, Eq. (4) is defined for times larger than $t_2 = 36.0$ s (power supply off) and represents an exponential decay of the temperature from an upper limit T_{max} to a final temperature T_f after long times τ_c ($\tau_c \gg \tau_2$).

As shown in Fig. 9, two exponential models [Eqs. (3) and (4)] were applied for representing the evolution of the sample and diamond temperatures in order to get quantitative results about the typical time constants of the present internally heated DAC system.

The time dependence of the sample temperature shown in Fig. 9(c) was reproduced along the heating ramp by Eq. (3), floating the time constant τ_1. The initial temperature T_0 was kept fixed as $T_0 = 298$ K, and also the final temperature T_{limit} was fixed to the known asymptotic limit ($T_{limit} = 1534$ K, as obtained by the power-temperature calibration curve shown in Fig. 2). The resulting best-fit time constant was found to be $\tau_1 = 10.17$ s (with a typical 10% uncertainty), and the best-fit (green) curve is in good agreement with the data, as shown in Fig. 9(c). Heating rates at constant power then can reach typical values of 100 K/s at the onset reducing to about 20 K/s in the thermalization process.

A similar procedure was applied for reproducing the time evolution of the sample temperature upon cooling. In this case, we have used $T_{max} = 1469.2$ K for the upper limit (at time t_2, as expected by above exponential heating ramp), while both T_f and τ_2 were allowed to float. The best-fit was obtained for $T_f = 480$ K and $\tau_2 = 7.85$ s (typical uncertainty 15%). Typical cooling rates of 150 K/s can be reached at the onset of the decay region, while the thermalization process proceeds much slower at longer times.

The exponential models of Eqs. (3) and (4) have been successfully applied also for temperature evolution in the diamond anvils. In this case, exponential trends are observed for both heating and cooling, and the entire temporal domain can be used to refine the time constants. The heating process was described by fixing the initial temperature to $T'_0 = 298$ K and floating two parameters: the temperature limit T'_{limit} and the time constant τ'_1. The quality of the fit in the 6 s–36 s time interval [shown as a green curve in Fig. 9(e)] is nice, and the resulting best-fit values were $T'_{limit} = 1317.5$ K and $\tau'_1 = 10.4$ s (typical uncertainty 5%). The temperature evolution upon cooling ($t > t_2 = 36$ s) was accurately reproduced using the exponential decay [Eq. (4)], floating two parameters T'_f and τ'_2, for a given value of $T'_{max} = 1260.4$ K (boundary condition at time $t_2 = 36$ s). The agreement with the experimental data is remarkably good for final best-fit values $T'_f = 347.7$ K and $\tau'_2 = 9.34$ s (typical uncertainty 5%). It is possible to see from the asymptotic rising profile in Fig. 9 [green curves in Figs. 9(c) and 9(d)] that for a given step-like increase in power, the sample and diamond temperatures approach thermal equilibrium within typically ~60 s.

It is interesting to remark that the time constants related to the sample and diamond temperatures are similar although the heating process is slightly faster and more efficient in the sample region.

However, minor temporal delays and temperature shifts are reasonable and expected due the larger size of the diamond anvils, their high thermal conductivity, and the direct contact with the colder DAC components (anvil seats).

Generally speaking, the results of kinetic XAS experiments demonstrated interesting capabilities of present the high temperature DAC system for time-resolved experiments with heating and cooling rates in the 100 K/s regime. This internally heated DAC is therefore particularly suited for dynamical experiments with sub-second time resolution in the moderate high temperature (up to 1500 K) range. We have performed many fast isobaric thermal cycles at different heating/cooling rates in the pressure range up to 10 GPa and in the temperature range up to 1800 K (see the supplementary material for additional data), and we did not experience any failure with the diamond anvils. Heating and cooling rates can be tuned changing the amount of the supplied power (final temperature T_{limit}) and also by changing the power profile from a simple square wave (as in the present experiment) to suitable saw-teeth or more complex functions using possible options in modern power-supply devices.

According to our experience, the heater design presented here can be safely used for high temperature high pressure experiments up to 1500 K and 20 GPa and may also be extended further depending on the culet dimension of the diamond anvils and preventing chemical reactions.

V. CONCLUSIONS

We have presented the design and performances of a new internally heated DAC system. In this device, the gasket design allowed us to use it both for sample confinement and as the heating element, eliminating several complications related to the sample assembly in internally heatable DAC. Moreover, the design was conceived to reduce the size of the heating spot near the sample region, obtaining a corresponding reduction in the needed electric power and an improvement in heating and cooling performances. A suitable compact vacuum chamber allowing for a variety of *in situ* x-ray and optical experiments has been also presented and put to a test in applications.

The new internally heated DAC has been widely tested under high temperature high pressure conditions by performing several thermal emission and optical spectroscopy measurements. A robust relationship between electric power and local sample temperature has been established up to 1500 K by a measurement campaign on different simple substances. In particular, thermal emission and ruby fluorescence measurements were performed using a micro-Raman spectrometer suitably calibrated for this purpose. Good spatial resolution of the micro-Raman system was used to measure the temperature distribution of the sample that resulted to be uniform within the typical uncertainty of these measurements (5% at 1000 K).

High-quality XAS measurements of germanium at 3.5 GPa were obtained in the 300 K–1300 K range, studying the melting transition and nucleation to the crystal phase. The achievable heating and cooling rates of the DAC were studied with sub-second time resolution exploiting the XAS dispersive setup at the ODE beamline.[22] An original dynamical XAS temperature calibration procedure, based on the edge energy shift and on the occurrence of diamond glitches, was used to monitor the sample and diamond temperatures. Temperature variations were successfully described using simple exponential models with typical time constants in the 10 s range. We have thus verified that heating and cooling rates in the 100 K/s range can be easily achieved using this device. Heating and cooling rates can be tuned for different kinetic experiments by suitable adjustments of the power–time profiles.

SUPPLEMENTARY MATERIAL

See the supplementary material for more information about the design of the DAC and vacuum chamber, thermal emission measurements, and additional kinetic XAS measurements.

ACKNOWLEDGMENTS

This work was performed within an agreement between the School of Advanced Studies of the University of Camerino and the Soleil Synchrotron, and Y.M. thanks the two institutions for supporting this research (Ph.D. grant). The authors are grateful to Leonardo Properzi who contributed in the initial part of this work and Alain Polian for his constant support at Soleil. They would also like to thank Carlo Checchi and Romain Ciurko for their useful advices. They thank Yan Huacai, Wei Xiangjun, and Liu Zhen for their help during part of the XAS measurements. They also thank Li Wenlin for his help in data-analysis. They acknowledge Synchrotron SOLEIL for provision of beamtime and the University of Camerino for the use of micro-Raman and other laboratory equipments. They also thank Dr. Toru Shinmei and acknowledge the support of PRIUS Project No. 2019-B37 by the Joint Usage/Research Center PRIUS, Ehime University, Japan.

DATA AVAILABILITY

The data that support the findings of this study are available from the corresponding author upon reasonable request.

REFERENCES

[1] T. Katsura, K.-i. Funakoshi, A. Kubo, N. Nishiyama, Y. Tange, Y.-i. Sueda, T. Kubo, and W. Utsumi, Phys. Earth Planet. Inter. **143-144**, 497 (2004), part of Special Issue: New Developments in High-Pressure Mineral Physics and Applications to the Earth's Interior.
[2] S. Zhai and E. Ito, Geosci. Front. **2**, 101 (2011).
[3] A. Dewaele, P. Loubeyre, F. Occelli, O. Marie, and M. Mezouar, Nat. Commun. **9**, 2913 (2018).
[4] Z. Jenei, E. O'Bannon, S. Weir, H. Cynn, M. Lipp, and W. Evans, Nat. Commun. **9**, 3563 (2018).
[5] N. Dubrovinskaia, L. Dubrovinsky, N. A. Solopova, A. Abakumov, S. Turner, M. Hanfland, E. Bykova, M. Bykov, C. Prescher, V. B. Prakapenka *et al.*, Sci. Adv. **2**, e1600341 (2016).
[6] P. Loubeyre, F. Occelli, and R. LeToullec, Nature **416**, 613 (2002).
[7] E. Ito and E. Takahashi, Nature **328**, 514 (1987).
[8] A. Filipponi, M. Borowski, D. T. Bowron, S. Ansell, A. Di Cicco, S. De Panfilis, and J.-P. Itiè, Rev. Sci. Instrum. **71**, 2422 (2000).
[9] G. Morard, M. Mezouar, N. Rey, R. Poloni, A. Merlen, S. Le Floch, P. Toulemonde, S. Pascarelli, A. San-Miguel, C. Sanloup *et al.*, High Pressure Res. **27**, 223 (2007).

[10]A. Di Cicco and A. Filipponi, in *X-Ray Absorption Spectroscopy of Semiconductors*, Springer Series in Optical Sciences Vol. 190, edited by C. S. Schnohr and M. C. Ridgway (Springer Berlin Heidelberg, 2015), pp. 187–200.
[11]A. D. Rosa, J. Pohlenz, C. de Grouchy, B. Cochain, Y. Kono, S. Pasternak, O. Mathon, T. Irifune, and M. Wilke, High Pressure Res. **36**, 332 (2016).
[12]S. Tateno, K. Hirose, Y. Ohishi, and Y. Tatsumi, Science **330**, 359 (2010).
[13]G. Aquilanti, A. Trapananti, A. Karandikar, I. Kantor, C. Marini, O. Mathon, S. Pascarelli, and R. Boehler, Proc. Natl. Acad. Sci. U. S. A. **112**, 12042 (2015).
[14]G. Shen, L. Wang, R. Ferry, H.-k. Mao, and R. J. Hemley, J. Phys.: Conf. Ser. **215**, 012191 (2010).
[15]R. Boehler, H. G. Musshoff, R. Ditz, G. Aquilanti, and A. Trapananti, Rev. Sci. Instrum. **80**, 045103 (2009).
[16]L. R. Benedetti and P. Loubeyre, High Pressure Res. **24**, 423 (2004).
[17]L.-c. Ming and W. A. Bassett, Rev. Sci. Instrum. **45**, 1115 (1974).
[18]D. L. Heinz and R. Jeanloz, J. Geophys. Res.: Solid Earth **92**, 011437, https://doi.org/10.1029/jb092ib11p11437 (1987).
[19]G. Shen, M. L. Rivers, Y. Wang, and S. R. Sutton, Rev. Sci. Instrum. **72**, 1273 (2001).
[20]V. B. Prakapenka, A. Kubo, A. Kuznetsov, A. Laskin, O. Shkurikhin, P. Dera, M. L. Rivers, and S. R. Sutton, High Pressure Res. **28**, 225 (2008).
[21]A. F. Goncharov, V. B. Prakapenka, V. V. Struzhkin, I. Kantor, M. L. Rivers, and D. A. Dalton, Rev. Sci. Instrum. **81**, 113902 (2010).
[22]F. Baudelet, Q. Kong, L. Nataf, J. D. Cafun, A. Congeduti, A. Monza, S. Chagnot, and J. P. Itié, High Pressure Res. **31**, 136 (2011).
[23]D. Schiferl, Rev. Sci. Instrum. **58**, 1316 (1987).
[24]Z. Jenei, H. Cynn, K. Visbeck, and W. J. Evans, Rev. Sci. Instrum. **84**, 095114 (2013).
[25]H.-P. Liermann, S. Merkel, L. Miyagi, H.-R. Wenk, G. Shen, H. Cynn, and W. J. Evans, Rev. Sci. Instrum. **80**, 104501 (2009).
[26]S. Pasternak, G. Aquilanti, S. Pascarelli, R. Poloni, B. Canny, M.-V. Coulet, and L. Zhang, Rev. Sci. Instrum. **79**, 085103 (2008).
[27]Z. Du, L. Miyagi, G. Amulele, and K. K. M. Lee, Rev. Sci. Instrum. **84**, 024502 (2013).
[28]L. S. Dubrovinsky, S. K. Saxena, and P. Lazor, Geophys. Res. Lett. **24**, 1835, https://doi.org/10.1029/97gl01746 (1997).
[29]J. a. Xu and E. Huang, Rev. Sci. Instrum. **65**, 204 (1994).
[30]N. M. Balzaretti, E. J. Gonzalez, G. J. Piermarini, and T. P. Russell, Rev. Sci. Instrum. **70**, 4316 (1999).
[31]N. Ishimatsu, N. Kawamura, M. Mizumaki, H. Maruyama, H. Sumiya, and T. Irifune, High Pressure Res. **36**, 381 (2016).
[32]Y. Mijiti, A. Trapananti, M. Minicucci, M. Ciambezi, J. Coquet, L. Nataf, F. Baudelet, and A. D. Cicco, Radiat. Phys. Chem. **175**, 108106 (2018).
[33]A. Filipponi and A. Di Cicco, Nucl. Instrum. Methods Phys. Res., Sect. B **93**, 302 (1994).
[34]A. D. Cicco, B. Giovenali, R. B. E. Principi, and E. Principi, Phys. Scr. **T115**, 1068 (2005).
[35]A. D. Rosa, M. Merkulova, G. Garbarino, V. Svitlyk, J. Jacobs, C. J. Sahle, O. Mathon, M. Munoz, and S. Merkel, High Pressure Res. **36**, 564 (2016).
[36]D. Antonangeli, T. Komabayashi, F. Occelli, E. Borissenko, A. C. Walters, G. Fiquet, and Y. Fei, Earth Planet. Sci. Lett. **331-332**, 210 (2012).
[37]F. Datchi, A. Dewaele, P. Loubeyre, R. Letoullec, Y. Le Godec, and B. Canny, High Pressure Res. **27**, 447 (2007).
[38]F. Coppari, A. Di Cicco, E. Principi, A. Trapananti, N. Pinto, A. Polian, S. Chagnot, and A. Congeduti, High Pressure Res. **30**, 28 (2010).
[39]Y. Waseda, *Liquids and Amorphous Solids* (McGraw-Hill, 1980).
[40]A. Filipponi and A. Di Cicco, Phys. Rev. B **51**, 12322 (1995).
[41]P. Lautenschlager, P. B. Allen, and M. Cardona, Phys. Rev. B **31**, 2163 (1985).
[42]P. Jacobson and S. Stoupin, Diamond Relat. Mater. **97**, 107469 (2019).